ATMOSPHERIC SCIENCE

Typhoon-boosted biogenic emission aggravates cross-regional ozone pollution in China

Nan Wang[1,2], Xin Huang[1,3,4]*, Jiawei Xu[1], Tong Wang[1], Zhe-min Tan[1], Aijun Ding[1,3,4]*

Ozone pollution that threatens human health and the ecosystem is a global environmental challenge. In megacities, ozone pollution has long been mainly attributed to anthropogenic sources. However, the processes and mechanisms of cross-regional transport of ozone and its precursors under interactions between mixed sources remain unclear. Here, we show that Northwest Pacific typhoons could intensify the chemical interactions between anthropogenic and biogenic emissions, resulting in extreme ozone pollution in two main city clusters in China. By integrating field and satellite observations together with model simulations, we show that biogenic emission and cross-regional ozone transport are greatly enhanced by approaching typhoons, with the increments reaching up to 78.0 and 22.5%, respectively. Ozone formation efficiency has more than doubled because of abundant precursors and active photochemistry. This study highlights the importance of natural emissions in areas with intensive human activity, which needs to be considered in future air pollution control in China.

INTRODUCTION

Ground-level ozone (O_3) is an air pollutant that poses detrimental impacts on human health and crop productivity (*1*–*4*). O_3 also drives the production of the hydroxyl radical, which controls the photochemical lifetime of many atmospheric pollutants and reactive greenhouse gases (*5*–*9*). As a secondary pollutant, tropospheric O_3 is predominantly formed in situ by photochemical reactions involving nitrogen oxides (NO_x) and volatile organic compounds (VOCs) (*7*, *10*–*12*). Thus, quantitatively understanding the sources and formation process of O_3 is of great importance for the mitigation policy of air pollution.

Emissions of NO_x are dominated by anthropogenic combustion processes, whereas VOCs originate from both human activities and biogenic emissions especially from forest ecosystems (*5*, *13*–*16*). Severe O_3 pollution and its deterioration have long been attributed to intensive anthropogenic activities (*6*, *17*, *18*). However, despite that strict measures have been widely implemented to cut down anthropogenic emissions in the past decades, increases in ground-level O_3 pollution have been witnessed in many places of the Northern Hemisphere (*19*, *20*). The highest O_3 concentrations and largest increment predominantly concentrate in the mid-latitude (*21*), particularly evident in China. Specifically, O_3 pollution days in China are 93 to 575% more than other industrialized countries, jeopardizing the health of the world's largest population (*22*).

Meteorological parameters including incident sunlight and air temperature modulate the O_3 formation, accumulation, and transport (*13*, *23*, *24*). The extreme O_3 pollution generally outbreaks in summer and has been proven to be closely linked to high air temperature and strong solar radiation together with stagnant weather conditions (*24*–*28*). Recent observations have identified O_3 mixing ratios in cities of eastern China well in excess of present air quality standards under the influence of Northwest Pacific typhoon, a frequent weather activity in warm seasons (*29*–*33*). Because of the fact that the typhoon weather is highly variable and the precursor emissions in this region are very complex, quantitatively understanding O_3 pollution under this circumstance is particularly challenging. Here, using in situ and satellite observations and chemical transport model for 6 years from 2013 to 2018, we provide a quantitative assessment of how the Northwest Pacific typhoon leads to these extreme O_3 pollution events in eastern China and also disentangle the key factors that control O_3 production and its transport under this unique environment.

RESULTS

Aggravating O_3 pollution in city clusters associated with approaching typhoons

China's O_3 features highest levels in summer with 90th percentile of maximum daily 8-hour average (MDA8) of O_3 concentration reaching up to approximately 90 parts per billion (ppb) (*5*, *34*). Summer and autumn are also the seasons when China is subject to the most frequent typhoon activities in the Western Pacific. Long-term measurements from 2013 to 2018 in Fig. 1A and fig. S1 indicate that, under the typhoon-associated weather systems, O_3 pollution would get even worse, especially in two most densely populated city clusters—Yangtze River Delta (YRD) region and Pearl River Delta (PRD) region. Quantitatively, MDA8 O_3 concentrations in these two regions rise by 28.3 and 53.8%, respectively, under the influence of typhoons, comparing to the summertime climatology. Shanghai and Guangzhou, the two largest megacities located in YRD and PRD, respectively, have witnessed 30.3- and 39.1-ppb high anomalies as typhoons approach. Such an O_3 increment is particularly remarkable when typhoon tracks are nearby the island of Taiwan. Even more noteworthily, O_3 soars in succession with YRD polluted a few days earlier (Fig. 1, C and D).

The coastal eastern and southern China, including both YRD and PRD, is characterized by a very typical subtropical monsoon climate and western pacific subtropical high (WPSH) in summer (*35*–*37*). The intervention of a typhoon tends to weaken and stretch westward WPSH (Fig. 1B). The change in large-scale circulation and synoptic weather is highly sensitive to the specific position of typhoon (*38*). To understand the typhoon tracks in the Western Pacific, we applied

[1]School of Atmospheric Sciences, Nanjing University, Nanjing 210023, China. [2]Institute of Tropical and Marine Meteorology/Guangdong Provincial Key Laboratory of Regional Numerical Weather Prediction, China Meteorological Administration, Guangzhou 510640, China. [3]Collaborative Innovation Center for Climate Change, Jiangsu Province, Nanjing 210023, China. [4]Frontiers Science Center for Critical Earth Material Cycling, Nanjing University, Nanjing 210023, China.
*Corresponding author. Email: xinhuang@nju.edu.cn (X.H.); dingaj@nju.edu.cn (A.D.)

an objective method to classify typhoons in the past decade. It is found that typhoons passing by Taiwan are the most conducive ones, bringing about O_3 pollution episodes in both YRD and PRD city clusters (Fig. 1, C and D, and figs. S2 and S3). This kind of typhoon notably weakens the subtropical high, retracting the WPSH around 30°N (Fig. 1, C and D, and fig. S4) and greatly modifying the weather system in both regions. As the typhoons reshape the circulation, O_3 pollution starts to cover YRD and PRD in succession. Statistically, the typhoon-induced O_3 pollution features two distinct phases, that is, O_3 pollution tends to first deteriorate in YRD (the YRD phase) and then followed by PRD (the PRD phase) (Fig. 1, C and D, and fig. S5). Spatially, it is found that the YRD region is the first to suffer from severe O_3 pollution when the typhoon center is located around 15°N to 20°N. In the subsequent phase of PRD pollution, typhoon center ranges from 20°N to 25°N (fig. S5).

Typhoon-boosted biogenic emissions and cross-regional O_3 transport

The summertime extreme O_3 pollution in eastern China has been long attributed to fast photochemical production of intensive anthropogenic NO_x and VOC emissions under intense solar radiation (*13*, *20*, *27*). Moreover, southern China settles a large area of forest, just between YRD and PRD, which releases tremendous biogenic VOCs (BVOCs) as additional O_3 precursors (Fig. 1A) (*35*). The spatial heterogeneity of these O_3 precursors and nonlinearity of O_3 chemistry make the regional transport and mixing processes substantially modulate O_3 pollution. When a typhoon approaches, the circulation in eastern China shows great shift from the typical summer monsoon to prevailing northerly winds (Fig. 2, A and B), corresponded to the aforementioned YRD and PRD phases.

During the YRD phase, the mainland China prevails southeast wind, which is mainly affected by the summer monsoon system (Fig. 2A). The air flow is relatively clean for PRD as it comes from the South China Sea. Quite the reverse, the low-pressure system of the cyclone makes the WPSH move northward to the mid-latitude and then cover the YRD region, leading to a stagnant condition there. As the cyclonic center moves northwest, the external air flow of the typhoon sweeps the southern China, the mainland prevails northerly winds (Fig. 2B), and subsequently, PRD steps into pollution. The strong atmospheric subsidence of a typhoon periphery favors an intense solar radiation and stagnant condition. By comparing the meteorological conditions under the influence of typhoon with the summer average, it is clear that the noontime air temperature and incident solar radiation are increased by 4.6 K and 9.1 W/m^2, together with the noticeable drop of relative humidity in both YRD and PRD (Fig. 2, C to E). These parameters are all conducive to vigorous photochemistry and the resultant O_3 formation.

In addition, biogenic emission itself is also highly dependent on the meteorology (*15*, *39*). The broad area of forest in southern China does undergo marked variations under typhoon-associated weather system based on the meteorology-driven calculation using the Model of Emissions of Gases and Aerosols from Nature (MEGAN) (see Materials and Methods). Take the Typhoon Nesat in 2017 as an example, isoprene, the most abundant BVOC species (*15*, *40*), witnesses a remarkable rise of 94% over the forest area in southern China. Regarding the spatial distribution, isoprene emission enhancement

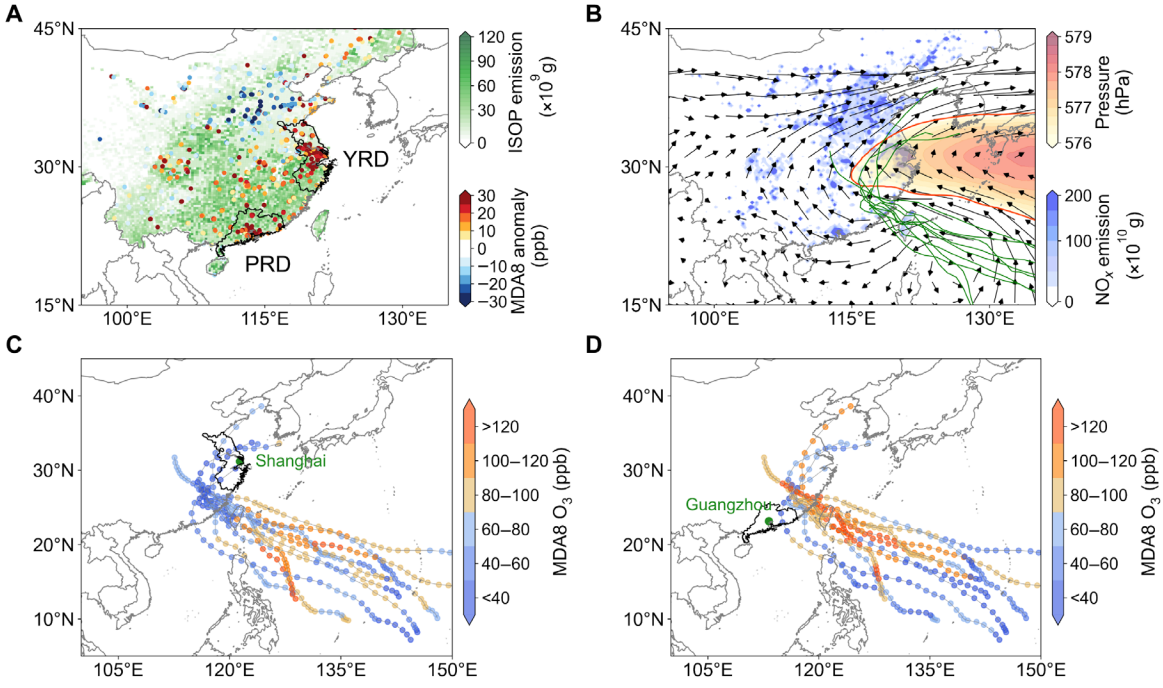

Fig. 1. Typhoon tracks and its associated abnormally high O_3 pollution in city clusters YRD and PRD. (**A**) MD8A O_3 concentration anomaly during typhoon-associated period compared with the summer average (dotted) from 2013 to 2018 and summer averaged isoprene (ISOP) emission calculated by MEGAN model. (**B**) Distribution of annual anthropogenic NO_x emissions (contoured with blue), averaged 500-hPa pressure (contoured with red), and wind based on ERA5 [ECMWF (European Centre for Medium-Range Weather Forecasts) Reanalysis v5] reanalysis data during the phase of YRD O_3 pollution. The solid red line highlights the position of WPSH, and the green lines show the tracks of historic typhoons crossing Taiwan. (**C**) Ninetieth percentile of MDA8 O_3 levels in YRD corresponding to the position of typhoon. (**D**) Same as (C) but for PRD.

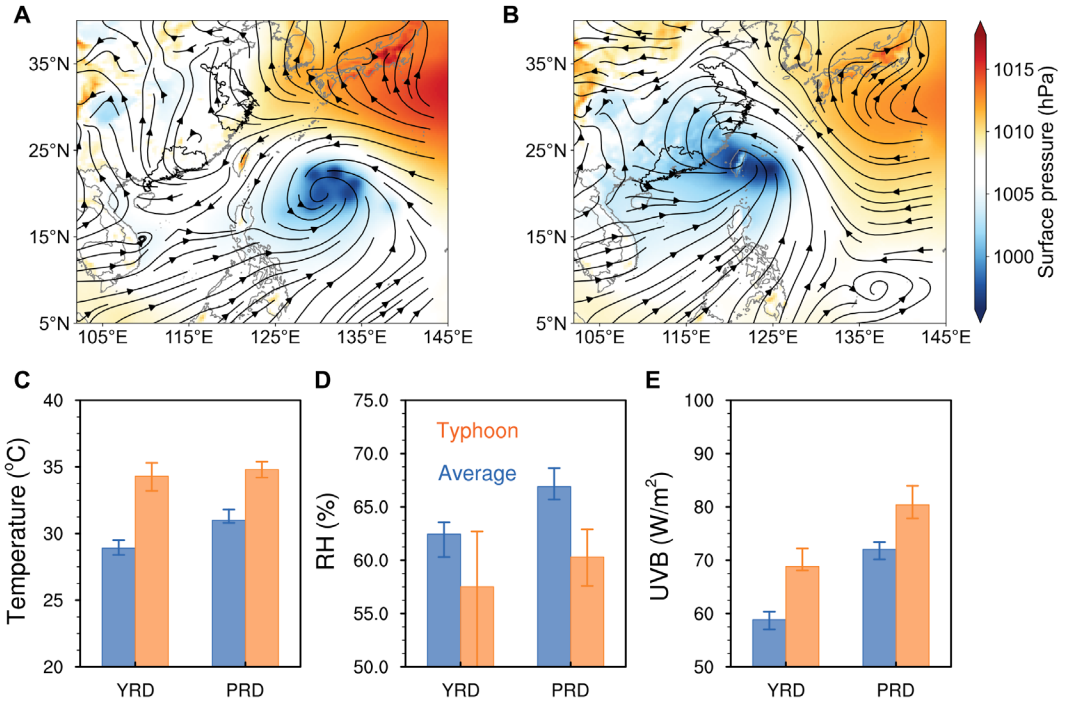

Fig. 2. Typhoon-modulated circulations and meteorological conditions at different ozone pollution phases. Averaged wind field and sea-level pressures showing the position of typhoon at the phase of YRD pollution (**A**) and PRD pollution (**B**), respectively. (**C** to **E**) Difference of 2-m temperature, relative humidity (RH), and incident ultraviolet radiation b (UVB) at 14:00 local time between typhoon-associated weather system and the summertime climatology in PRD and YRD, respectively.

is found in central China and the northern part of PRD during the YRD phase and in most areas of PRD and its adjoining northern areas during the PRD phase (Fig. 3, A and B). The significant increase in BVOC emissions correlates well with the rising air temperature, indicating the predominant impact of weather conditions (*16*, *38*). Statistically, the averaged isoprene emission of historical typhoon events from 2013 to 2018 is 78.0% greater than the summer climatology, providing solid evidence that BVOC emissions are prominently intensified by the typhoon-associated weather systems (Fig. 3D). To identify the impact of the enhanced BVOCs on O_3 pollution in city clusters, we further adopt the backward Lagrangian particle dispersion modeling (LPDM) to simulate the potential source region of air masses for YRD and PRD. The 48-hour backward potential source regions of YRD and PRD point to the high vegetable coverage area in the southern China (Fig. 3C). Considering the typical circulation of typhoon periphery, it is indicated that the intensified BVOCs are prone to be transported to city clusters with dense anthropogenic emission and contribute to O_3 pollution there.

Accelerated O_3 production by the interaction of anthropogenic and biogenic sources

In addition to meteorological variations, O_3 formation sensitivity regime features great regional disparities over the eastern China. As clearly demonstrated in fig. S6, in megacities with high NO_x environments like YRD and PRD, the formation of O_3 is typically VOC-limited, while the O_3 production over the forest area is highly sensitive to the ambient NO_x availability (*41*). In normal days without intense cross-regional transport in warm seasons, the urban emissions or biogenic emissions alone are insufficient to build up O_3 pollution as the production efficiency maintains at a relatively low level. Conversely, the typhoon-associated weather tends to intensely mix anthropogenic and biogenic emissions by strong rotational winds. To quantitatively understand the interactions therein, we conduct parallel simulations using chemical transport model Weather Research and Forecasting (WRF) coupled Community Multiscale Air Quality (CMAQ) (WRF-CMAQ) (see Materials and Methods). The modeling results reveal that typhoon-boosted BVOC emissions enhance photochemical reactions in city clusters with contributions to O_3 formations by more than 30 ppb in both regions. Because both the city clusters are in the VOC-limited or transitional regime, the intervention of BVOCs plays an "adding fuel" role in urban photochemical pollution. Specifically, O_3 pollution is enhanced by anthropogenic and biogenic interactions via two pathways. One is the reaction with primary biogenic emissions, especially isoprene near the ground surface. It is worth noting that the reactivity of BVOCs often doubles or even triples that of anthropogenic VOCs (*42*, *43*). Once released, isoprene reacts with atmospheric oxidants and subsequently generates O_3. This contribution is drastic near the ground surface, with the maxima contribution more than 30 ppb (Fig. 4, A and C). The other is via the reaction with the transported biogenic intermediate products, including methyl vinyl ketone, methacrolein, methyl glyoxal, etc., in the upper planetary boundary layer (PBL) even during nighttime (*44*). In general, isoprene itself predominately involves in local photochemistry due to its high reactivity; however, its intermediate product can be long-rangely transported hundreds of kilometers. The model results demonstrate that a huge amount of biogenic intermediate products inburst to downwind city clusters following typhoon circulation (fig. S7) reacts with local oxidants, such as OH radical and O_3 and NO_3 radicals, and then generates RO_2 radical, thereby enhancing O_3 by almost

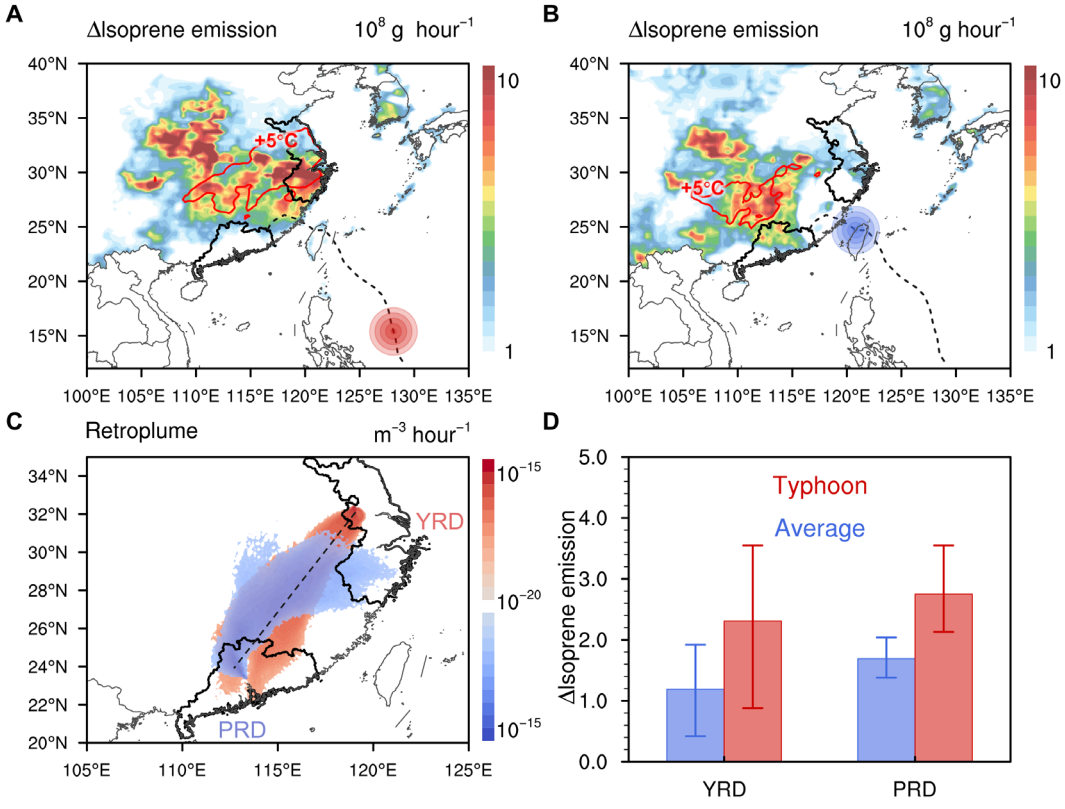

Fig. 3. Typhoon-boosted biogenic emissions and cross-regional O_3 transport in eastern China during Typhoon Nesat in 2017. (**A**) Spatial distribution of BVOC emission enhancement (contour) and 2-m air temperature anomaly (isolines) in the phase of YRD pollution while the Typhoon Nesat is approaching China. (**B**) Same as (A) but in the phase of PRD pollution. The dashed lines mark the track of the Typhoon Nesat, and the circles show the typhoon position at the corresponding phases. (**C**) Forty-eight–hour retroplume (footprint residence time) showing transport pathways of air masses at YRD and PRD during the two pollution phrases, respectively. (**D**) Comparisons of isoprene emissions during the historic typhoon periods from 2013 to 2018 and the summer average in YRD and PRD

10 ppb. Consequently, influenced by the intensified BVOC emissions, the downwind urban features an increase in O_3 formation efficiency by 126%, suffering from severe O_3 pollution.

Besides the vigorous interactions of BVOCs and anthropogenic emissions, cross-regional transport also matters because of the typical circulation of typhoon periphery. As shown in fig. S8, during the first phase (YRD pollution), intensive anthropogenic emission in PRD could substantially affect the downwind areas. The YRD region, even further away, is still influenced with O_3 contribution more than 10 ppb. As a secondary pollutant with relatively long lifetime, O_3 could be either directly transported or locally produced by precursors from upwind areas (*18*, *45*). Our modeling results indicate that photochemically produced O_3 from PRD emissions is mainly distributed locally, and hardly can the precursors from PRD be transported to YRD. Instead, it is the direct advection of O_3 in the upper PBL and daytime convective mixing that make O_3 enhancement in PRD greatly contribute to O_3 pollution in YRD (fig. S8, A and B). In the PRD phase, the outflow of typhoon dominates the southern China, and the prevailing wind becomes from YRD to PRD. The accumulated O_3 in YRD is, in turn, horizontally transported back and lastly influences PRD with a contribution more than 20 ppb (fig. S8C). By analyzing O_3 diurnal patterns along the transport pathway from tens of monitoring stations, the O_3 peaks depict a "lagging effect" from the upwind area to the downwind regions, which further supports the importance of cross-regional interaction based on direct in situ observations (fig. S9).

To identify the contribution of typhoon-enhanced O_3 pollution statistically, we then carried out the exactly same simulations for all the historical events from 2013 to 2018, as shown in fig. S10. By integrating the findings, we propose a conceptual scheme illustrating the enhancement of cross-regional O_3 pollution by typhoon-intensified anthropogenic and biogenic interaction and quantify the contributions from key factors in Fig. 5. As shown, NO_x and other pollutants first emitted in PRD pass the BVOC-concentrated forest area, and then the mixed anthropogenic and biogenic plume results in O_3 pollution when arriving YRD. In the second phase, pollutants accumulated in YRD are then swept back under the influence of typhoon outflow, passing the BVOC-concentrated forest area again, and give rise to PRD O_3 pollution. Comparisons of O_3 source apportionment between typhoon events and the summer average are analyzed using WRF-CMAQ (Fig. 4, B and D). In YRD, the contributions of BVOC emissions are significantly increased from 16.9 to 33.6%. The cross-regional transport by PRD anthropogenic emissions also increases from 4.8 to 8.2%. In terms of PRD pollution, the regional transport dominates O_3 formation with an increase from 31 to 53.5%, among which the YRD contribution increases by approximately five times from 1.7 to 9.9%. The contribution of BVOC emission also gets more vital, increasing from 16.9 to 26.6%.

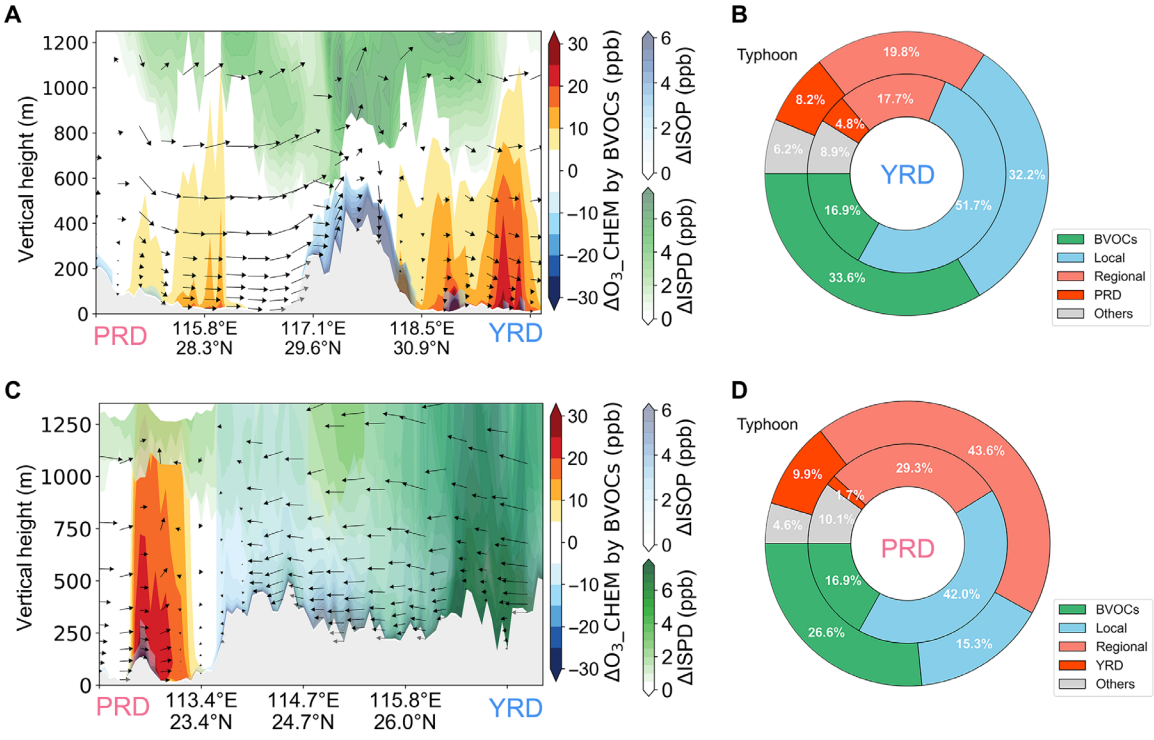

Fig. 4. Chemical interactions between anthropogenic emission and natural BVOCs accelerate O_3 formation under the influence of typhoon. (**A**) Cross section of wind field and BVOCs' impact on O_3 in YRD along the blue cross-regional transport pathway marked in Fig. 3C. The red contour shows the chemical contribution by BVOC emissions to O_3 formation. The blue contour shows isoprene concentrations by BVOC emissions. The green contour shows BVOC intermediate product (ISPD; lumped methacrolein, methyl vinyl ketone, methyl glyoxal, etc.) concentrations. (**B**) Source apportionment of O_3 formation in YRD. The inner pie shows the summer average, and the outer pie shows the typhoon-affected period. To be noted that the local, regional, PRD/YRD all refer to anthropogenic emissions. (**C**) Same as (A) but for PRD. (**D**) Same as (B) but for PRD.

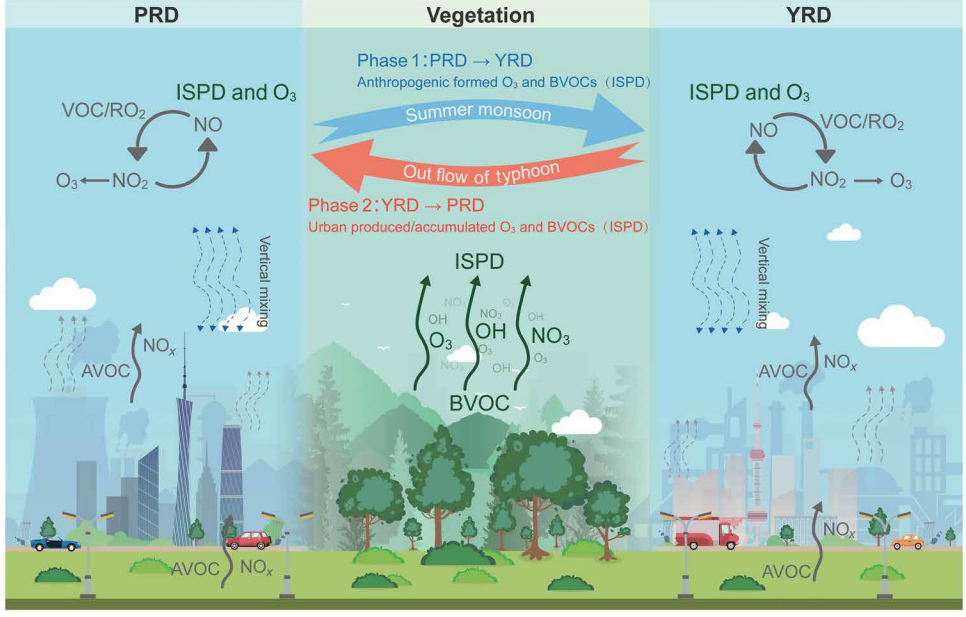

Fig. 5. Conceptual scheme illustrating how typhoon aggravates cross-regional ozone pollution in eastern China and quantitative assessment of key factors therein.

Because that it is the anthropogenic and biogenic interaction that greatly enhances O_3 pollution, we further explored the potential benefits of a precedent control of anthropogenic emission before typhoon in pollution mitigation by using the model tools (fig. S11). Promisingly, with the help of meteorology and air quality forecast, regional coordinated emission control in short term could help us to alleviate the O_3 enhancement due to approaching typhoons.

DISCUSSION

O_3 pollution features the nonlinear response to emission intensity and involves multiple precursors and is also greatly modulated by synoptic weather. Southern China, characterized by two emission-intensive city clusters and a broad vegetation coverage, provides a unique lens to dig into the interaction of biogenic and anthropogenic emissions, particularly under typhoon when O_3 pollution peaks. Our study shows that a typhoon-affected weather system is the trigger to intensify the natural emissions of BVOCs and creates favorable meteorological conditions for photochemical reactions. Furthermore, the circulation of typhoon periphery enhances cross-regional transport and interactions of anthropogenic and biogenic emissions, facilitating O_3 pollution in urban areas. This O_3 enhancement is expected in other regions featuring both mixed emissions and frequent typhoon or hurricane activity, like the southeastern United States and northern India (*46*, *47*). Our results emphasize the importance of natural sources on tropospheric O_3 pollution even in areas with dense anthropogenic activity and replenish the understanding on typhoon-intensified interactions of anthropogenic and biogenic emissions on tropospheric O_3 pollution. Even in highly polluted regions like eastern China, more consideration ought to be given to the coordinated cross-regional joint emission control. Moreover, the typhoon activities are strongly linked with climate variability and climate change (*48*, *49*), and biogenic emission could be also enhanced because of the global warming or carbon neutral–induced greening (*50*). Therefore, these interactions between biogenic and anthropogenic activities may be further intensified and play a more vital role in O_3 pollution in the future.

MATERIALS AND METHODS

Clustering of typhoon tracks with O_3 levels

Clustering analysis is introduced to distinguish historical typhoon tracks. Because the number of clusters is already known, *K*-means clustering method is used. This method classifies *n* points of data *X* into initializing *k* clusters

$$J = \sum_{k=1}^{K}\sum_{i=1}^{n}\|x_i - u_i\|^2$$

where *u* is the center points of an individual cluster and *J* is the minimum distance from every point to its center point. This classification is repeated until each cluster gets stable. This algorithm has been used in many aspects (*28*, *51*).

In this study, we collect 11-year historical typhoons (2008 to 2018) affecting China with a total number of 88 tracks. The clustering analysis lastly provides four types of tracks. O_3 network data obtained from China National Environmental Monitoring Centre (CNEMC) are integrated corresponding to the position of the typhoon. There are 42 monitoring sites distributed in YRD and 40 in PRD, respectively. The 90th percentile of MDA8 O_3 is used to represent the degree of O_3 pollution in a specific region. Because the O_3 network data are only available after 2013, we then integrate O_3 data with the classified tracks from 2013 to 2018.

Lagrangian particle dispersion modeling

LPDM was adopted with the aim to investigate the potential source region affecting air masses in YRD and PRD, respectively. Global Data Assimilation System (GDAS) data are used as the meteorological input, and the model is conducted using hybrid single-particle Lagrangian-integrated trajectory (HYSPLITY). In this study, we released 3000 particulates at 100 m over the receptor region, and the model was traced backward for 48 hours with a time resolution of 1 hour. After a calculation of mean wind and a turbulence transport component, the position of each particulate was identified in spatial. The footprint "retroplume," representing the distribution of the surface probability or the residence time of the simulated air mass, was used to identify the contribution from potential source regions.

MEGAN model

BVOC emissions by terrestrial ecosystems are estimated with the aid of MEGAN model (version 2.10). As a biogenic emission model, MEGAN can estimate global and regional BVOC emissions, with horizontal resolution ranging from 1 × 1 km to around 100 × 100 km. The model can estimate up to 146 BVOC species, for example, isoprene, monoterpene, sesquiterpene, and so on, and lump them according to a specific gas-phase chemistry mechanism. In this study, WRF-simulated results provide meteorological conditions including temperature, solar radiation, and relative humidity for MEGAN. Leaf area index and plant functional types retrieved from moderate resolution imaging spectroradiometer (MODIS) products are used to provide basic vegetation information. All the calculated BVOC species are mapped to Carbon Bond 05 (CB05) gas-phase mechanism. Major BVOC emissions, i.e., isoprene emissions, are identified and compared between typhoon-associated events and the summer averages.

Diagnosing O_3-NO*x*-VOC sensitivity by satellite retrievals

To illustrate the responses of O_3 to its precursors, the O_3-NO_x-VOC sensitivities are explored by using the ratios of satellite-retrieved formaldehyde (HCHO) and NO_2. Daily HCHO and NO_2 column densities are obtained from the resolution of the GOME-2 retrievals. The data control is based on the principle by previous studies (*52*). In this study, the area with HCHO/NO_2 ratio below 1 is considered as NO_x-saturated (VOC-limited) regime, the area with HCHO/NO_2 ratio above 2 is identified as the NO_x-limited regime, and the HCHO/NO_2 ratio between 1 and 2 indicates the mixed-limited regime (*53*).

WRF-CMAQ simulation

WRF (version 3.9.1) coupled CMAQ (version 5.0.2) model is applied to simulate O_3 and its precursors in southern China. The WRF model is driven by Final (FNL) Operational Global Analysis data. To better represent the meteorological conditions, the National Centers for Environmental Prediction (NCEP) Automated Data Processing Global Upper Air Observational Weather Data have been assimilated. The modeling system consists of two domains, with a grid resolution of 36 × 36 km and 12 × 12 km, respectively. The outer domain covers most part of East Asia; the inner domain mainly focuses on the eastern China. In vertical, there are 39 levels for all domains with the top at 100 hpa and ~20 levels within the boundary

layer. The chemical boundary and initial conditions for WRF-CMAQ model are derived from a global chemical model [MOZART-4 (Model for Ozone and Related chemical Tracers, version 4)]. Anthropogenic emission inventories are obtained from the Multi-resolution Inventory for China, which has a grid resolution of 0.25° and covers anthropogenic emissions from human activities of power plant, transportation, industry, agriculture, and residential. Natural emissions including BVOCs and soil-emitted NO are calculated using the MEGAN (version 2.10). The WRF-CMAQ spins up for 10 days before starting a simulation.

The key configurations of WRF-CMAQ include the Rapid Radiative Transfer Model (RRTM) for short- and long-wave radiation scheme, the Noah Land Surface Model for land-atmospheric interactions, the Yonsei University boundary layer scheme, the Lin microphysics scheme, the Kain-Fritsch scheme for cumulus parameterization, and the CB05 combined with AERO6 (aerosol 6 module) for gas-phase and aerosol chemistry, respectively.

The model performance is then validated by the comparisons with available observations. Statistical metrics are introduced, including the averages (Obs_{mean} and Sim_{mean}), mean bias (MB; $Obs_{mean} - Sim_{mean}$), normalized MB (NMB;$NMB = \sum_{i=1}^{n}[(Sim(i) - Obs(i))/Obs(i)]$), root mean square error (RMSE; $RMSE = \sqrt{\frac{1}{n}\sum_{i=1}^{n}(Sim(i) - Obs(i))^2}$), and the index of agreement (IOA; $IOA = 1 - \frac{\sum_{i=1}^{n}(Sim(i) - Obs(i))^2}{\sum_{i=1}^{n}(|Sim(i) - \overline{Obs}| + |Obs(i) - \overline{Obs}|)^2}$). The statistical results are summarized in table S1. In general, the evaluated results show that the WRF-CMAQ model can well reproduce the historical O_3 pollution events.

The integrated process rate (IPR) module in CMAQ is used to calculate the contributions from each individual physical and chemical process to O_3 formation. The considered atmospheric processes include the photochemical process (the net O_3 formation rate via gas-phase reactions), the horizontal transport (including horizontal convection and diffusion), the vertical a transport (including vertical convection and diffusion), the emissions, the deposition (including dry and wet deposition), and the cloud processes with the aqueous chemistry. The individual contribution is calculated at each time step during the simulation. In this work, we mainly use the technique to investigate the key photochemical species including O_3, CO, NO_x, anthropogenic VOCs, BVOCs, and the intermediate BVOC product.

To quantify all the individual impact of anthropogenic emissions and BVOC emissions to O_3 pollution, all the historical cases with typhoon crossing the Taiwan from 2013 to 2018 are simulated with WRF-CMAQ model. Parallel simulations are conducted under different emission scenarios. The scenarios include considering/excluding BVOC emissions, anthropogenic emissions of PRD, anthropogenic emissions of YRD, and anthropogenic emissions out of YRD and PRD. For example, to identify the impact from PRD anthropogenic emissions on YRD, parallel simulations are conducted with and without PRD anthropogenic emissions. Then, the difference in O_3 between the two simulations is identified as the impact from PRD anthropogenic emissions. The influence from the emissions within the region itself is considered as the local contribution; otherwise, the one out of the border is regarded as the regional transport. By using this method, O_3 source apportionment is analyzed during historical typhoon events and the summer season. Moreover, by combining with the IPR technique, the changes of net O_3 formation rate due to gas-phase reactions (including photochemically production and consumption processes) and atmospheric physical process (i.e., advective transport) driven by a given set of emissions are recorded at each time step. Accordingly, the individual impact of anthropogenic emissions and BVOCs on O_3 formation can be identified.

SUPPLEMENTARY MATERIALS

Supplementary material for this article is available at https://science.org/doi/10.1126/sciadv.abl6166

REFERENCES AND NOTES

1. A. S. Lefohn, C. S. Malley, L. Smith, B. Wells, M. Hazucha, H. Simon, V. Naik, G. Mills, M. G. Schultz, E. Paoletti, A. De Marco, X. Xu, L. Zhang, T. Wang, H. S. Neufeld, R. C. Musselman, D. Tarasick, M. Brauer, Z. Feng, H. Tang, K. Kobayashi, P. Sicard, S. Solberg, G. Gerosa, Tropospheric ozone assessment report: Global ozone metrics for climate change, human health, and crop/ecosystem research. *Elementa* **6**, 27 (2018).
2. A. P. K. Tai, M. V. Martin, C. L. Heald, Threat to future global food security from climate change and ozone air pollution. *Nat. Clim. Change* **4**, 817–821 (2014).
3. Z. Feng, E. Hu, X. Wang, L. Jiang, X. Liu, Ground-level O3 pollution and its impacts on food crops in China: A review. *Environ. Pollut.* **199**, 42–48 (2015).
4. G. P. Brasseur, P. Artaxo, L. A. Barrie, R. J. Delmas, I. Galbally, W. M. Hao, R. C. Harriss, I. S. A. Isaksen, D. J. Jacob, C. E. Kolb, M. Prather, H. Rodhe, D. Schwela, W. Steffen, D. J. Wuebbles, An integrated view of the causes and impacts of atmospheric changes. *Atmos. Chem. A Chang. World* **2003**, 207–230 (2003).
5. L. K. Xue, T. Wang, J. Gao, A. J. Ding, X. H. Zhou, D. R. Blake, X. F. Wang, S. M. Saunders, S. J. Fan, H. C. Zuo, Q. Z. Zhang, W. X. Wang, Ground-level ozone in four Chinese cities: Precursors, regional transport and heterogeneous processes. *Atmos. Chem. Phys.* **14**, 13175–13188 (2014).
6. D. T. Shindell, D. Rind, P. Lonergan, Increased polar stratospheric ozone losses and delayed eventual recovery owing to increasing greenhouse-gas concentrations. *Nature* **392**, 589–592 (1998).
7. D. J. Jacob, Heterogeneous chemistry and tropospheric ozone. *Atmos. Environ.* **34**, 2131–2159 (2000).
8. X. Huang, A. Ding, J. Gao, B. Zheng, D. Zhou, X. Qi, R. Tang, J. Wang, C. Ren, W. Nie, X. Chi, Z. Xu, L. Chen, Y. Li, F. Che, N. Pang, H. Wang, D. Tong, W. Qin, W. Cheng, W. Liu, Q. Fu, B. Liu, F. Chai, S. J. Davis, Q. Zhang, K. He, Enhanced secondary pollution offset reduction of primary emissions during COVID-19 lockdown in China. *Natl. Sci. Rev.* **8**, nwaa137 (2021).
9. M. Claeys, B. Graham, G. Vas, W. Wang, R. Vermeylen, V. Pashynska, J. Cafmeyer, P. Guyon, M. O. Andreae, P. Artaxo, W. Maenhaut, Formation of secondary organic aerosols through photooxidation of isoprene. *Science* **303**, 1173–1176 (2004).
10. G.-J. Roelofs, J. Lelieveld, Distribution and budget of O_3 in the troposphere calculated with a chemistry general circulation model. *J. Geophys. Res.* **100**, 20983–20998 (1995).
11. M. E. Jenkin, K. C. Clemitshaw, Chapter 11 Ozone and other secondary photochemical pollutants: Chemical processes governing their formation in the planetary boundary layer. *Dev. Environ. Sci.* **1**, 285–338 (2002).
12. S. M. Aschmann, J. Arey, R. Atkinson, OH radical formation from the gas-phase reactions of O_3 with a series of terpenes. *Atmos. Environ.* **36**, 4347–4355 (2002).
13. T. Wang, L. Xue, P. Brimblecombe, Y. F. Lam, L. Li, L. Zhang, Ozone pollution in China: A review of concentrations, meteorological influences, chemical precursors, and effects. *Sci. Total Environ.* **575**, 1582–1596 (2017).
14. P. M. Edwards, S. S. Brown, J. M. Roberts, R. Ahmadov, R. M. Banta, J. A. DeGouw, W. P. Dubé, R. A. Field, J. H. Flynn, J. B. Gilman, M. Graus, D. Helmig, A. Koss, A. O. Langford, B. L. Lefer, B. M. Lerner, R. Li, S. M. Li, S. A. McKeen, S. M. Murphy, D. D. Parrish, C. J. Senff, J. Soltis, J. Stutz, C. Sweeney, C. R. Thompson, M. K. Trainer, C. Tsai, P. R. Veres, R. A. Washenfelder, C. Warneke, R. J. Wild, C. J. Young, B. Yuan, R. Zamora, High winter ozone pollution from carbonyl photolysis in an oil and gas basin. *Nature* **514**, 351–354 (2014).
15. A. Guenther, T. Karl, P. Harley, C. Wiedinmyer, P. I. Palmer, C. Geron, Estimates of global terrestrial isoprene emissions using MEGAN (Model of Emissions of Gases and Aerosols from Nature). *Atmos. Chem. Phys.* **6**, 3181–3210 (2006).
16. W. L. Chameides, R. W. Lindsay, J. Richardson, C. S. Kiang, The role of biogenic hydrocarbons in urban photochemical smog: Atlanta as a case study. *Science* **241**, 1473–1475 (1988).
17. Y. Zhang, O. R. Cooper, A. Gaudel, A. M. Thompson, P. Nédélec, S.-Y. Ogino, J. J. West, Tropospheric ozone change from 1980 to 2010 dominated by equatorward redistribution of emissions. *Nat. Geosci.* **9**, 875–879 (2016).
18. J. Ou, Z. Huang, Z. Klimont, G. Jia, S. Zhang, C. Li, J. Meng, Z. Mi, H. Zheng, Y. Shan, P. K. K. Louie, J. Zheng, D. Guan, Role of export industries on ozone pollution and its precursors in China. *Nat. Commun.* **11**, 5492 (2020).

19. A. Gaudel, O. R. Cooper, G. Ancellet, B. Barret, A. Boynard, J. P. Burrows, C. Clerbaux, P.-F. Coheur, J. Cuesta, E. Cuevas, S. Doniki, G. Dufour, F. Ebojie, G. Foret, O. Garcia, M. J. Granados-Muñoz, J. W. Hannigan, F. Hase, B. Hassler, G. Huang, D. Hurtmans, D. Jaffe, N. Jones, P. Kalabokas, B. Kerridge, S. Kulawik, B. Latter, T. Leblanc, E. Le Flochmoën, W. Lin, J. Liu, X. Liu, E. Mahieu, A. M. Clure-Begley, J. L. Neu, M. Osman, M. Palm, H. Petetin, I. Petropavlovskikh, R. Querel, N. Rahpoe, A. Rozanov, M. G. Schultz, J. Schwab, R. Siddans, D. Smale, M. Steinbacher, H. Tanimoto, D. W. Tarasick, V. Thouret, A. M. Thompson, T. Trickl, E. Weatherhead, C. Wespes, H. M. Worden, C. Vigouroux, X. Xu, G. Zeng, J. Ziemke, Tropospheric Ozone Assessment Report: Present-day distribution and trends of tropospheric ozone relevant to climate and global atmospheric chemistry model evaluation. *Elementa* **6**, 39 (2018).
20. K. Li, D. J. Jacob, H. Liao, L. Shen, Q. Zhang, K. H. Bates, Anthropogenic drivers of 2013–2017 trends in summer surface ozone in China. *Proc. Natl. Acad. Sci. U.S.A.* **116**, 422–427 (2019).
21. O. R. Cooper, D. D. Parrish, J. Ziemke, N. V. Balashov, M. Cupeiro, I. E. Galbally, S. Gilge, L. Horowitz, N. R. Jensen, J. F. Lamarque, V. Naik, S. J. Oltmans, J. Schwab, D. T. Shindell, A. M. Thompson, V. Thouret, Y. Wang, R. M. Zbinden, Global distribution and trends of tropospheric ozone: An observation-based review. *Elementa* **2**, 000029 (2014).
22. Y. Li, Y. Xue, J. Guang, L. She, C. Fan, G. Chen, Ground-level $PM_{2.5}$ concentration estimation from satellite data in the Beijing area using a specific particle swarm extinction mass conversion algorithm. *Remote Sens. (Basel)* **10**, 1906 (2018).
23. L. Xue, A. Ding, O. Cooper, X. Huang, W. Wang, D. Zhou, Z. Wu, A. McClure-Begley, I. Petropavlovskikh, M. O. Andreae, C. Fu, ENSO and Southeast Asian biomass burning modulate subtropical trans-Pacific ozone transport. *Natl. Sci. Rev.* **8**, nwaa132 (2021).
24. A. Ding, T. Wang, M. Zhao, T. Wang, Z. Li, Simulation of sea-land breezes and a discussion of their implications on the transport of air pollution during a multi-day ozone episode in the Pearl River Delta of China. *Atmos. Environ.* **38**, 6737–6750 (2004).
25. M. Lin, L. W. Horowitz, Y. Xie, F. Paulot, S. Malyshev, E. Shevliakova, A. Finco, G. Gerosa, D. Kubistin, K. Pilegaard, Vegetation feedbacks during drought exacerbate ozone air pollution extremes in Europe. *Nat. Clim. Change* **10**, 444–451 (2020).
26. A. Russo, R. M. Trigo, H. Martins, M. T. Mendes, NO2, PM10 and O3 urban concentrations and its association with circulation weather types in Portugal. *Atmos. Environ.* **89**, 768–785 (2014).
27. N. Wang, J. Xu, C. Pei, R. Tang, D. Zhou, Y. Chen, M. Li, X. Deng, T. Deng, X. Huang, A. Ding, Air Quality during COVID-19 lockdown in the yangtze river delta and the pearl river delta: Two different responsive mechanisms to emission reductions in China. *Environ. Sci. Technol.* **55**, 5721–5730 (2021).
28. J. Xu, X. Huang, N. Wang, Y. Li, A. Ding, Understanding ozone pollution in the Yangtze River Delta of eastern China from the perspective of diurnal cycles. *Sci. Total Environ.* **752**, 141928 (2021).
29. C. Y. Chan, L. Y. Chan, Effect of meteorology and air pollutant transport on ozone episodes at a subtropical coastal Asian city, Hong Kong. *J. Geophys. Res. Atmos.* **105**, 20707–20724 (2000).
30. L. Shu, M. Xie, T. Wang, D. Gao, P. Chen, Y. Han, S. Li, B. Zhuang, M. Li, Integrated studies of a regional ozone pollution synthetically affected by subtropical high and typhoon system in the Yangtze River Delta region, China. *Atmos. Chem. Phys.* **16**, 15801–15819 (2016).
31. X. Wei, K. S. Lam, C. Cao, H. Li, J. He, Dynamics of the typhoon haitang related high ozone episode over Hong Kong. *Adv. Meteorol.* **2016**, 1–12 (2016).
32. J.-P. Huang, J. C. H. Fung, A. K. H. Lau, Y. Qin, Numerical simulation and process analysis of typhoon-related ozone episodes in Hong Kong. *J. Geophys. Res. Atmos.* **110**, D05301 (2005).
33. M. Ying, W. Zhang, H. Yu, X. Lu, J. Feng, Y. X. Fan, Y. Zhu, D. Chen, An overview of the China meteorological administration tropical cyclone database. *J. Atmos. Oceanic Tech.* **31**, 287–301 (2014).
34. X. Lu, J. Hong, L. Zhang, O. R. Cooper, M. G. Schultz, X. Xu, T. Wang, M. Gao, Y. Zhao, Y. Zhang, Severe surface ozone pollution in China: A global perspective. *Environ. Sci. Technol. Lett.* **5**, 487–494 (2018).
35. X. Wang, F. Chen, Z. Wu, M. Zhang, M. Tewari, A. Guenther, C. Wiedinmyer, Impacts of weather conditions modified by urban expansion on surface ozone: Comparison between the Pearl River Delta and Yangtze River Delta regions. *Adv. Atmos. Sci.* **26**, 962–972 (2009).
36. J. Zhang, Y. Gao, K. Luo, L. Ruby Leung, Y. Zhang, K. Wang, J. Fan, Impacts of compound extreme weather events on ozone in the present and future. *Atmos. Chem. Phys.* **18**, 9861–9877 (2018).
37. L. Chang, J. Xu, X. Tie, W. Gao, The impact of climate change on the Western Pacific subtropical high and the related ozone pollution in Shanghai, China. *Sci. Rep.* **9**, 16998 (2019).
38. C. Zhan, M. Xie, C. Huang, J. Liu, T. Wang, M. Xu, C. Ma, J. Yu, Y. Jiao, M. Li, S. Li, B. Zhuang, M. Zhao, D. Nie, Ozone affected by a succession of four landfall typhoons in the Yangtze River Delta, China: Major processes and health impacts. *Atmos. Chem. Phys.* **20**, 13781–13799 (2020).
39. M. Ma, Y. Gao, Y. Wang, S. Zhang, L. Ruby Leung, C. Liu, S. Wang, B. Zhao, X. Chang, H. Su, T. Zhang, L. Sheng, X. Yao, H. Gao, Substantial ozone enhancement over the North China Plain from increased biogenic emissions due to heat waves and land cover in summer 2017. *Atmos. Chem. Phys.* **19**, 12195–12207 (2019).
40. J. Zheng, Z. Zheng, Y. Yu, L. Zhong, Temporal, spatial characteristics and uncertainty of biogenic VOC emissions in the Pearl River Delta region, China. *Atmos. Environ.* **44**, 1960–1969 (2010).
41. S. Situ, A. Guenther, X. Wang, X. Jiang, A. Turnipseed, Z. Wu, J. Bai, X. Wang, Impacts of seasonal and regional variability in biogenic VOC emissions on surface ozone in the Pearl river delta region, China. *Atmos. Chem. Phys.* **13**, 11803–11817 (2013).
42. W. P. L. Carter, Condensed atmospheric photooxidation mechanisms for isoprene. *Atmos. Environ.* **30**, 4275–4290 (1996).
43. X. Xie, M. Shao, Y. Liu, S. Lu, C. C. Chang, Z. M. Chen, Estimate of initial isoprene contribution to ozone formation potential in Beijing, China. *Atmos. Environ.* **42**, 6000–6010 (2008).
44. S. S. Brown, W. P. Dubé, Y. J. Tham, Q. Zha, L. Xue, S. Poon, Z. Wang, D. R. Blake, W. Tsui, D. D. Parrish, T. Wang, Nighttime chemistry at a high altitude site above Hong Kong. *J. Geophys. Res. Atmos.* **121**, 2457–2475 (2016).
45. R. A. Cox, A. E. J. Eggleton, R. G. Derwent, J. E. Lovelock, D. H. Pack, Long-range transport of photochemical ozone in north-western Europe. *Nature* **255**, 118–121 (1975).
46. K. Sindelarova, C. Granier, I. Bouarar, A. Guenther, S. Tilmes, T. Stavrakou, J.-F. Müller, U. Kuhn, P. Stefani, W. Knorr, Global data set of biogenic VOC emissions calculated by the MEGAN model over the last 30 years. *Atmos. Chem. Phys.* **14**, 9317–9341 (2014).
47. N. Bloemendaal, I. D. Haigh, H. de Moel, S. Muis, R. J. Haarsma, J. C. J. H. Aerts, Generation of a global synthetic tropical cyclone hazard dataset using STORM. *Sci. Data.* **7**, 40 (2020).
48. Y.-P. Guo, Z.-M. Tan, Westward migration of tropical cyclone rapid-intensification over the Northwestern Pacific during short duration El Niño. *Nat. Commun.* **9**, 1507 (2018).
49. H. Lee, C.-S. Jin, D.-H. Cha, M. Lee, D.-K. Lee, M.-S. Suh, S.-Y. Hong, H.-S. Kang, Future change in tropical cyclone activity over the western north pacific in CORDEX-East Asia Multi-RCMs Forced by HadGEM2-AO. *J. Climate* **32**, 5053–5067 (2019).
50. H. Wang, Q. Wu, A. B. Guenther, X. Yang, L. Wang, T. Xiao, J. Li, J. Feng, Q. Xu, H. Cheng, A long-term estimation of biogenic volatile organic compound (BVOC) emission in China from 2001-2016: The roles of land cover change and climate variability. *Atmos. Chem. Phys.* **21**, 4825–4848 (2021).
51. A. Ahmad, L. Dey, A k-mean clustering algorithm for mixed numeric and categorical data. *Data Knowl. Eng.* **63**, 503–527 (2007).
52. I. De Smedt, J. F. Müller, T. Stavrakou, R. Van Der A, H. Eskes, M. Van Roozendael, Twelve years of global observations of formaldehyde in the troposphere using GOME and SCIAMACHY sensors. *Atmos. Chem. Phys.* **8**, 4947–4963 (2008).
53. X. Jin, T. Holloway, Spatial and temporal variability of ozone sensitivity over China observed from the Ozone Monitoring Instrument. *J. Geophys. Res. Atmos.* **120**, 7229–7246 (2015).

Acknowledgments

Funding: This work was funded by National Natural Science Foundation of China (41725020, 41805131, and 41922038) and Fundamental Research Funds for the Central Universities of China (DLTD2107). **Author contributions:** Conceptualization: A.D. and X.H. Methodology: N.W., X.H., and J.X. Investigation: N.W., X.H., T.W., and Z.T. Visualization: N.W. and X.H. Supervision: A.D. and X.H. Writing—original draft: N.W. and X.H. Writing—review and editing: N.W., X.H., Z.T., and A.D. **Competing interests:** The authors declare that they have no competing interests. **Data and materials availability:** Historical typhoon track data are obtained from the Tropical Cyclone Data Center of the China Meteorological Administration, available at http://tcdata.typhoon.org.cn. O_3 concentration at the monitoring network is obtained from CNEMC (www.cnemc.cn/). Daily HCHO and NO_2 column densities from the GOME-2 retrievals are openly accessible at https://earth.esa.int/eogateway/instruments/gome. ERA5 meteorological parameters are obtained at www.ecmwf.int/en/forecasts/datasets/reanalysis-datasets/era5. Global operational global analysis data and upper air observational weather data can be obtained at https://rda.ucar.edu/datasets/ds083.2 and https://rda.ucar.edu/datasets/ds351.0. The MEIC emission inventories are available at www.meicmodel.org. All data needed to evaluate the conclusions in the paper are present in the paper and/or the Supplementary Materials. The observation and simulation data supporting the main findings of this study are available at figshare data publisher (https://doi.org/10.6084/m9.figshare.16709095).

Submitted 25 July 2021
Accepted 22 November 2021
Published 14 January 2022
10.1126/sciadv.abl6166

ScienceAdvances

Typhoon-boosted biogenic emission aggravates cross-regional ozone pollution in China

Nan WangXin HuangJiawei XuTong WangZhe-min TanAijun Ding

Sci. Adv., 8 (2), eabl6166. • DOI: 10.1126/sciadv.abl6166

Science Advances (ISSN) is published by the American Association for the Advancement of Science. 1200 New York Avenue NW, Washington, DC 20005. The title *Science Advances* is a registered trademark of AAAS.